Conference paper

Michel Herm*, Xavier Gaona, Thomas Rabung, David Fellhauer, Claire Crepin, Kathy Dardenne, Marcus Altmaier* and Horst Geckeis

Solubility and spectroscopic study of An^{III}/Ln^{III} in dilute to concentrated Na–Mg–Ca–Cl–NO_3 solutions

Abstract: The complexation of An^{III}/Ln^{III} with nitrate was investigated in dilute to concentrated Na–Mg–Ca–Cl–NO_3 solutions at $2.94 \leq pH_m \leq 13.2$ and $T = 22 \pm 2$ °C. Comprehensive solubility experiments with $Nd(OH)_3(s)$ were performed from undersaturation conditions and complemented by extensive spectroscopic studies using Cm(III)–TRLFS (time resolved laser fluorescence spectroscopy) and Nd–L_{III} EXAFS (extended X-ray absorption fine structure) under analogous pH_m, I_m and $m_{NO_3^-}$ conditions. Solid phases recovered from batch solubility experiments were characterized by XRD and SEM-EDS. A significant influence of nitrate on the solubility of $Nd(OH)_3(s)$ is observed in concentrated weakly alkaline $MgCl_2$–$Mg(NO_3)_2$ solutions with total salt concentration ≥ 2.83 m and $m_{NO_3^-} \geq 1.13$ m. Nitrate has no effect in any of the studied NaCl–$NaNO_3$ and $CaCl_2$–$Ca(NO_3)_2$ mixtures, thus highlighting the key role of Mg^{2+} in the Nd(III)–NO_3 interaction. The formation of inner-sphere complexes with the participation of Mg^{2+} is further confirmed by Cm(III)–TRLFS and Nd–L_{III} EXAFS. Based on these experimental evidences, the proposed chemical model includes the definition of two new aqueous species $Mg[An^{III}/Ln^{III}NO_3OH]^{3+}$ and $Mg[An^{III}/Ln^{III}NO_3(OH)_2]^{2+}$ in equilibrium with solid $Nd(OH)_3(s)$ and allows to derive the thermodynamic and activity models (Pitzer) for the system Nd^{3+}/Cm^{3+}–H^+–Mg^{2+}–OH^-–Cl^-–NO_3^-–H_2O.

Keywords: curium; EXAFS; ISSP-16; neodymium; nitrate; Pitzer model; quaternary complexes; solubility; TRLFS; weak complexation.

DOI 10.1515/pac-2014-1205

Introduction

A reliable prediction of the chemical behavior of actinides in aqueous solutions is necessary in performance assessment analysis of deep geological nuclear waste repositories. Although geological or geo-technical barrier systems may prevent or hinder formation water from contacting the waste, intrusion of aqueous solu-

Article note: A collection of invited papers based on presentations at the 16th International Symposium on Solubility Phenomena and Related Equilibrium Processes (ISSP-16), Karlsruhe, Germany, July 21–25 2014.

***Corresponding authors: Michel Herm and Marcus Altmaier,** Karlsruhe Institute of Technology, Institute for Nuclear Waste Disposal, P.O. Box 3640, 76021 Karlsruhe, Germany, e-mail: michel.herm@kit.edu (M.H.); marcus.altmaier@kit.edu (M.A.)
Xavier Gaona, Thomas Rabung, David Fellhauer, Kathy Dardenne and Horst Geckeis: Karlsruhe Institute of Technology, Institute for Nuclear Waste Disposal, P.O. Box 3640, 76021 Karlsruhe, Germany
Claire Crepin: Ecole National Supérieure de Chimie de Montpellier, 8 Rue de l'Ecole Normale, 34296 Montpellier CEDEX 5, France

tions into a repository has to be taken into account for several scenarios on the long-term evolution of a repository. At a depth of several hundreds of meters, relevant argillaceous and granitic type formation waters are Na^+/Cl^- type solutions, characterized by anaerobic conditions and a pH in the range of 7 to almost 9 [1]. Sedimentary and crystalline rock type formation waters are normally characterized by low ionic strength, although formation waters with elevated ionic strength are also found in sedimentary bedrocks in the Canadian Shield [2] and Cretaceous argillites in Northern Germany [3], among other examples. Fluid inclusions and brine pockets in rock salt formations are characterized by high ionic strength (I_m > 5 m) dominated by high concentrations of mainly Na^+, Mg^{2+}, K^+ and Cl^-. Corrosion of cementitious waste forms in $MgCl_2$ dominated brines may lead to high $CaCl_2$ concentrations (≥2 M) and highly alkaline pH_m (≈12) conditions [4].

High concentrations of nitrate (≥1 M) are expected in wastes from nuclear fuel reprocessing, although other sources/processes can be also responsible for elevated nitrate concentration/inventory in repositories for waste disposal [5, 6]. In the Waste Isolation Pilot Plant (WIPP), a deep underground salt mine for transuranic waste disposal (New Mexico, USA), the initial quantity of nitrate in waste is calculated to 2.74×10^7 mol [7]. Very high nitrate concentrations in combination with hyperalkaline pH conditions are also expected in several waste tanks of the Hanford Site (Washington, USA) [8]. Slow nitrate reduction kinetics expected at 25 °C and moderate H_2 partial pressure [9] may affect the aqueous speciation of radionuclides and thus impact their mobilization into the biosphere.

Reducing conditions develop after the closure of a deep underground repository for nuclear waste disposal due to anoxic iron/steel container corrosion, producing dissolved Fe(II) species, Fe(II)/Fe(III) phases and hydrogen. In these reducing geochemical conditions, actinides are expected to prevail in the tri- and tetravalent redox states. Although the aqueous chemistry of $An^{III/IV}$ under repository-relevant conditions is dominated by hydrolysis reactions under absence of other strongly complexing ligands, the interaction of actinides with salt brines leads to unique geochemical boundary conditions affecting significantly actinide solubility and speciation [10]. A number of recent studies have shown the formation of hitherto unknown ternary Ca–An–OH complexes in alkaline $CaCl_2$ brines accompanied with an increase in $An^{III/IV}$ solubility [11–14]. The formation of complexes with other inorganic or organic ligands can also impact the behavior of actinides and promote its mobilization into the biosphere.

The last update book released within the OECD Nuclear Energy Agency – thermochemical database project (NEA-TDB) [15] selected only thermodynamic data for the complex $AmNO_3^{2+}$, whereas no selection was provided for the system Pu(III)–NO_3. Recent Cm(III)–TRLFS studies with nitrate concentrations up to 4.61 m proposed the formation of $CmNO_3^{2+}$ and $Cm(NO_3)_2^+$ complexes and provided both lg β° and $\Delta_r H^\circ$ data [16, 17]. So far all these studies focused on acidic conditions, leaving aside the assessment of nitrate effects under neutral to alkaline, repository relevant pH conditions.

The interaction of nitrate with metal cations is considered to be weak, but slightly stronger than in the corresponding chloride systems [10, 18, 19]. A challenge in the modelling of these systems arises from the distinction between formation of (weak) complexes and variations in the activity coefficients [19, 20]. Usually, large changes of the ionic medium are necessary to study weak complex formation, which additionally cause changes of the activity coefficients of the species involved. Note that the NEA-TDB guidelines for the extrapolation to zero ionic strength discourages the replacement of more than 10 % of the background electrolyte by the ligand when assessing the formation of weak complexes [20]. Besides classical solution chemistry studies, the use of advanced spectroscopic techniques can help in the identification of new aqueous species, and thus provide key inputs in the definition of correct chemical models for complex systems.

This study aims at providing a comprehensive thermodynamic description of An^{III}/Ln^{III}–NO_3 interaction under repository-relevant pH conditions in the absence of carbonate and $T = 22 \pm 2$ °C. For this purpose, extensive batch solubility experiments were conducted with Nd(III) in dilute to concentrated NaCl–$NaNO_3$, $MgCl_2$–$Mg(NO_3)_2$ and $CaCl_2$–$Ca(NO_3)_2$ mixed solutions. Complementary spectroscopic measurements [Cm(III)–TRLFS, Nd–L_{III} EXAFS] and a detailed solid phase characterization (XRD, SEM-EDS) were performed to gain detailed insights into the aqueous speciation and solid phases prevailing in the studied systems. The combination of these approaches allows the development of chemical, thermodynamic and Pitzer activity models for the system Nd^{3+}/Cm^{3+}–H^+–Mg^{2+}–OH^-–Cl^-–NO_3^-–H_2O. Considering the widely accepted chemical analogy

between $Nd^{III}/Cm^{III}/Am^{III}/Pu^{III}$, this study provides the basis for an accurate assessment of the behavior of trivalent actinides in nitrate-rich wastes under repository-relevant conditions.

Experimental

Chemicals

All solutions were prepared with ultrapure water, purified with a Milli-Q academic apparatus (Millipore, 18.2 MΩ·cm, 22 ± 2 °C, pore size 0.22 µm) and purged several hours with Ar before use. NaCl (p.a.), $NaNO_3$ (p.a.), $MgCl_2{\cdot}6H_2O$ (p.a.), $Mg(NO_3)_2{\cdot}6H_2O$ (p.a.), $CaCl_2{\cdot}2H_2O$ (p.a.), $Ca(NO_3)_2{\cdot}4H_2O$ (p.a.), portlandite [$Ca(OH)_2$(cr), p.a.], $C_8H_{17}NO_3S$ (CHES, p.a.), $C_8H_{18}N_2O_4S$ (HEPES, p.a.), HCl (Titrisol®) and NaOH (Titrisol®) were obtained from Merck, $C_4H_{11}NO_3/C_4H_{11}NO_3{\cdot}HCl$ (TRIS/TRIS·HCl, p.a.) from Sigma-Aldrich, whereas brucite ($Mg(OH)_2$(cr), BioUltra > 99 %) was purchased from Fluka. $Nd(OH)_3$(s) was prepared by hydration of crystalline Nd_2O_3(cr) (p.a., Merck) in pure water under argon atmosphere. The complete solid phase transformation was confirmed by XRD (PDF 70-0215) [13, 21]. Mg-oxychloride [$Mg_2(OH)_3Cl{\cdot}4H_2O$(cr)] was synthesized by transformation of brucite in concentrated $MgCl_2$ solutions (≥2.5 M) as described in [22].

A 2×10^{-5} M Cm(III) stock solution in 0.1 M $HClO_4$ was used for TRLFS experiments. The isotopic composition of curium was 89.7 % Cm–248, 9.4 % Cm–246, 0.4 % Cm–243, 0.3 % Cm–244, 0.1 % Cm–245 and 0.1 % Cm–247.

pH measurements

The molal H^+ concentration ($pH_m = -\lg m_{H^+}$) was determined with combination pH electrodes (type Orion Ross, Thermo Scientific). Calibration against pH (activity scale) standard buffers (pH 6–12, Merck) yields operational "measured" pH_{exp} values in salt solutions of ionic strength $I_m > 0.1$ m, with $pH_m = pH_{exp} + A_m$. The empirical parameter A_m includes the individual activity coefficient γ_{H^+} and a contribution ΔE_j entailing the difference in liquid junction potential E_j between dilute pH buffer solutions for calibration and samples with high concentration of background electrolyte. Empirical A_m values for NaCl, $MgCl_2$ and $CaCl_2$ systems were previously reported elsewhere [11, 22]. A_m values of pure nitrate systems and nitrate-chloride mixtures were experimentally determined in the present work with standard solutions containing 2×10^{-2}–6.25×10^{-4} M HCl in 0.1–6.02 m NaCl–$NaNO_3$, 0.25–5.24 m $MgCl_2$–$Mg(NO_3)_2$ and 2.91/4.02 m $CaCl_2$–$Ca(NO_3)_2$ mixtures.

A_m values determined for NaCl–$NaNO_3$, $MgCl_2$–$Mg(NO_3)_2$ and $CaCl_2$–$Ca(NO_3)_2$ solutions are provided in Figure 1 and Table 1, together with A_m values available for NaCl, $MgCl_2$ and $CaCl_2$ systems as reported in literature [22]. A_m values for the different Cl^-–NO_3^- mixtures considered in this work were based on linear correlation with total NO_3^- concentration.

Nd(III) solubility and solid phase characterization

All samples were stored and prepared in argon glove boxes under exclusion of oxygen (O_2 < 5 ppm, $T = 22 \pm 2$ °C) and CO_2. All solutions were prepared volumetrically and the resulting molar concentrations were converted into the molal scale with the density values calculated using Pitzer equations with data reported elsewhere [23, 24]. Batch solubility experiments of Nd(III) were performed from undersaturation conditions with $Nd(OH)_3$(s) as solid phase in Polyvials® (HDPE, Zinsser Analytic). Five series of solubility experiments were prepared with different total salt concentrations of NaCl–$NaNO_3$ (0.1–6.02 m) and $MgCl_2$–$Mg(NO_3)_2$ (0.25–5.24 m) mixtures, whereas only two series were prepared in the case of $CaCl_2$–$Ca(NO_3)_2$ (2.85 and 4.02 m) mixtures (see Table 2). Na^+, Mg^{2+} and Ca^{2+} concentrations were fixed within series of constant

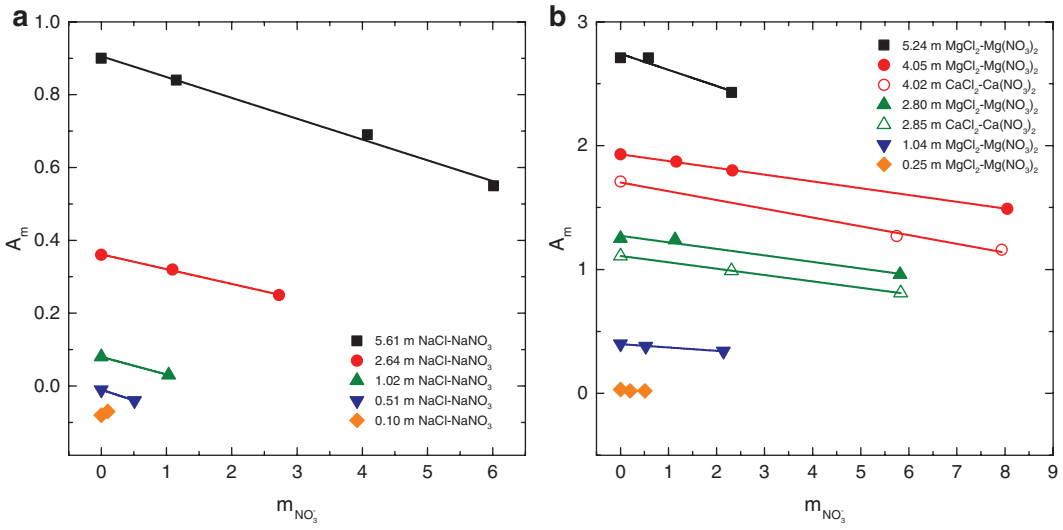

Fig. 1: A_m values experimentally determined for different (a) $NaCl–NaNO_3$, (b) $MgCl_2–Mg(NO_3)_2$ (closed symbols) and $CaCl_2–Ca(NO_3)_2$ (open symbols) mixtures as a function of the nitrate concentration. A_m values for $m_{NO_3^-} = 0$ are included in the figures as reported elsewhere [22]. Due to solubility limitations, nitrate concentration in the 5.24 m $MgCl_2–Mg(NO_3)_2$ series was kept ≤2.32 m.

Table 1: Equations empirically determined in this work for the calculation of A_m values in $NaCl–NaNO_3$, $MgCl_2–Mg(NO_3)_2$ and $CaCl_2–Ca(NO_3)_2$ mixtures.

System	Equation	System	Equation
m_{Na^+}		$m_{Mg^{2+}}$	
0.10	$A_m = +0.0994 \cdot m_{NO_3^-} - 0.0800$	0.25	$A_m = -0.0181 \cdot m_{NO_3^-} + 0.0276$
0.51	$A_m = -0.0590 \cdot m_{NO_3^-} - 0.0100$	1.04	$A_m = -0.0272 \cdot m_{NO_3^-} + 0.3975$
1.02	$A_m = -0.0484 \cdot m_{NO_3^-} + 0.0800$	2.80	$A_m = -0.0528 \cdot m_{NO_3^-} + 1.2722$
2.64	$A_m = -0.0406 \cdot m_{NO_3^-} + 0.3616$	4.05	$A_m = -0.0548 \cdot m_{NO_3^-} + 1.9306$
5.61	$A_m = -0.0572 \cdot m_{NO_3^-} + 0.9057$	5.24	$A_m = -0.1302 \cdot m_{NO_3^-} + 2.7424$
$m_{Ca^{2+}}$			
2.85	$A_m = -0.0514 \cdot m_{NO_3^-} + 1.1095$		
4.02	$A_m = -0.0708 \cdot m_{NO_3^-} + 1.7029$		

ionic strength and the concentrations of Cl^- and NO_3^- were varied according to a fixed pattern (see Table 2). Nitrate concentrations ranged between 0 and 8.0 m per batch solubility experiment. The solubility of nitrate in the series 5.24 m $MgCl_2–Mg(NO_3)_2$ was limited to $m_{NO_3^-} \leq 2.32$ m. For each ionic strength and Cl^-/NO_3^- mixture, a set of (at least) three independent samples was prepared within $7.5 \leq pH_m \leq 13.2$, with 15 mL background electrolyte and 6–12 mg $Nd(OH)_3(s)$. The pH in the samples was adjusted by the addition of organic buffers (150 µL 1.0 M HEPES (pH 7.5–7.9), TRIS (pH 8.3–8.4) or CHES (pH 8.6–10.0) to reach a final buffer concentration of 10 mM in the samples), brucite/Mg-oxychloride, portlandite, HCl and NaOH. The impact of these organic buffers on An^{III}/Ln^{III} speciation was evaluated in a previous study [25]. The solubility of brucite/Mg-oxychloride constrain the pH_m within a range of 8.6 and 9.1 depending upon $MgCl_2$ and nitrate concentration [22]. In the calcium system, portlandite buffers the pH_m to ~12. The pH_m controlled by these solid phases is denoted as "pH_{max}" for $MgCl_2–Mg(NO_3)_2$ and $CaCl_2–Ca(NO_3)_2$ systems in the following.

The pH and $m_{Nd(III)}$ were systematically monitored up to 398 days. Nd(III) concentration in the aqueous solution was determined by ICP-MS (X-Series II, Thermo Scientific) after 10 kD (~1.5 nm) ultrafiltration (Pall Life Sciences). Detection limit for Nd(III) is typically in the range of $10^{-9}–10^{-10}$ M depending on background electrolyte concentration in the sample and required dilution steps. The analytical uncertainties of the ICP-MS

Table 2: Summary of the matrix solutions used in the Nd(III) batch solubility experiments.

m_{Na^+}[a]	m_{NaCl}/m_{NaNO_3} or $m_{MCl2}/m_{M(NO_3)_2}$ with M = Mg^{2+} or Ca^{2+}									
0.10	0.10/0.00	0.00/0.10								
0.51	0.51/0.00	0.40/0.10	0.30/0.20	0.00/0.51						
1.02	1.02/0.00	0.92/0.10	0.82/0.20	0.51/0.51	0.00/1.03					
2.64	2.64/0.00	2.57/0.11	2.47/0.21	2.16/0.54	1.63/1.09		0.00/2.72			
5.61	5.61/0.00	5.61/0.11	5.50/0.23	5.17/0.57	4.61/1.15	3.48/2.32	2.90/2.90	1.75/4.08	0.00/6.02	
$m_{Mg^{2+}}$[a]										
0.25	0.25/0.00	0.20/0.05	0.15/0.10							
1.04	1.04/0.00	0.99/0.05	0.94/0.10	0.79/0.26	0.53/0.53	0.00/1.07				
2.80[b]	2.80/0.00	2.75/0.06	2.70/0.11	2.54/0.28	2.27/0.57	1.72/1.14			0.00/2.91	
4.05[b]	4.05/0.00	4.00/0.06	3.94/0.12	3.77/0.29	3.49/0.58	2.91/1.16			1.16/2.90	0.00/4.02
5.24[c]	5.24/0.00	5.19/0.06	5.13/0.12	4.95/0.29	4.65/0.58	4.05/1.16				
$m_{Ca^{2+}}$[a]										
2.85	2.85/0.00		2.74/0.11	2.57/0.29	2.30/0.57	1.73/1.16				
4.02									1.15/2.87	
$m_{NO_3^-}$[a]	0.00	0.10	0.20	0.51	1.03	2.14	2.72	4.08	5.74	8.04

At least three independent samples prepared for each mixed system within $7.5 \leq pH_m \leq 13.2$ (Na^+), $7.5 \leq pH_m \leq 9.0$ (Mg^{2+}) and $7.5 \leq pH_m \leq 12.0$ (Ca^{2+}).

[a]Axis labels refer to the lowest salt/nitrate concentration within a series/group.

[b]Additional pH_{max} series buffered with brucite instead of Mg-oxychloride.

[c]Samples with $m_{NO_3^-} > 2.32$ m were found to be sparingly soluble.

analyses are 5–10 %. The outcome of these solubility studies was compared with previous solubility experiments in nitrate-free NaCl, $MgCl_2$ and $CaCl_2$ solutions [13].

After ensuring equilibrium conditions (constant pH and $m_{Nd(III)}$), about 2 mg of Nd(III) solid phase recovered from selected batch experiments by centrifugation were characterized by X-ray diffraction (XRD). Although equilibria were typically obtained within a few days, XRD were taken after >79 days. Powder samples were washed four times with ethanol to remove the background electrolyte which can interfere in the XRD analysis, resuspended in approximately 20 µL ethanol and placed on a single crystal silicon waver.

XRD measurements were performed using a D8 Advance diffractometer (Bruker AXS) equipped with a Cu radiation tube, Ni filter and a Sol-X detector, working at an X-ray source current of 25 mA and a voltage of 40 kV. Diffractograms were recorded in the range $5° \leq 2\Theta \leq 60°$ with a step size of 0.04° 2Θ, 6 s counting time per step and variable slit widths. Measured reflexes were compared to XRD patterns of relevant phases of the JCPDS database [26].

A small fraction of the washed powder was further characterized by scanning electron microscope – energy-dispersive X-ray spectrometry (SEM-EDS). SEM-EDS analyses were carried out using a Quanta 650 FEG instrument (FEI) equipped with a Thermo Scientific UltraDry silicon drift X-ray detector. SEM images were collected at an electron acceleration voltage of 20 kV, whereas SEM-EDS measurements were done at 30 kV. Data analysis was performed using the NORAN System 7 X-ray microanalysis system for the Quanta 650 FEG instrument.

Nd–L_{III} EXAFS studies in $MgCl_2$–$Mg(NO_3)_2$ solutions

EXAFS measurements were conducted on the supernatant of a solubility sample taken from the 4.05 m $MgCl_2$–$Mg(NO_3)_2$. The sample was characterized by $m_{NO_3^-} = 5.81$ m, $pH_m = 8.15$ and $m_{Nd(III)} = 1.49 \times 10^{-3}$ m and was measured after 10 kD (~1.5 nm) ultrafiltration to avoid the contribution of colloidal species in the EXAFS spectra. The sample was prepared in a 400 µL polyethylene vial, double-sealed in a plastic envelop inside an Ar-glovebox and transported to the beamline.

Nd–L_{III} edge X-ray absorption fine structure (XAFS) spectra were recorded at the INE Beamline for Actinide and Radionuclide Science at ANKA. Spectra were energy calibrated to the first inflection point in the XANES spectra of a Mn metal foil (6.539 keV), which was measured simultaneously. The XAFS signal was recorded

at room temperature in fluorescence mode using a vortex Si-drift detector. Si<111> crystals were used in the double crystals monochromator, operating in fixed-exit mode. The parallel alignment of the crystal faces was detuned to ~70 % of the maximum beam intensity at the beginning of each scan. The incident intensity was then held constant by means of a piezo-driven feedback system to the second crystal.

EXAFS fits were performed with D-Artemis, a program of the Demeter IFEFFIT package [27], using phase and amplitude data calculated for a 59 atom cluster (~5.8 Å diameter sized centered on the individual metal cations). Feff6L delivered as standard with the package was replaced by Feff8.4 for these calculations. For magnesium atoms, single path scattering files for phase and amplitude were used. The k-range used in the modelling was [2.45–9.6 $Å^{-1}$]. Fits were performed in the R-space [1.25–4.5 Å] using simultaneously the k^1-, k^2- and k^3-weighted data. The structures used as model to fit to the data are $Nd(OH)_2NO_3$ [ICSD 63550] [28] and $Nd(NO_3)_3(H_2O)_4(H_2O)_2$ [ICSD 37181] [29].

Cm(III)–TRLFS studies

Time resolved laser fluorescence spectroscopy (TRLFS) measurements were performed with 1×10^{-7} M Cm(III) per sample with 5.61/6.02 m NaCl–$NaNO_3$, 0.25/4.05 m $MgCl_2$–$Mg(NO_3)_2$ and 4.02 m $CaCl_2$–$Ca(NO_3)_2$ as background electrolyte, containing 0–8.0 m NO_3^-. The pH_m in both $MgCl_2$–$Mg(NO_3)_2$ series was buffered to pH_{max} with brucite and Mg-oxychloride, respectively. In addition samples in 4.05 m $MgCl_2$–$Mg(NO_3)_2$ were further titrated to pH_m = 2.94 with 0.1 M HCl (of same ionic strength and composition). Samples in 5.61/6.02 m NaCl–$NaNO_3$ and 4.02 m $CaCl_2$–$Ca(NO_3)_2$ were buffered with TRIS or CHES to $7.93 \leq pH_m \leq 8.95$.

TRLFS measurements were performed using a Nd:YAG laser (Surelite II Laser, Continuum) pumping a dye laser (Narrowscan Dye Laser, Radiant Dyes). The repetition rate of the Nd:YAG laser was 10 Hz, with a maximum laser energy of 2 mJ. To filter out Rayleigh- and Raman scattering, as well as short-lived background fluorescence, the emission spectra were recorded in a range of 570–630 nm with a delay of 1 µs and in a time window of 1 ms. Emission spectra of each sample were integrated over 500 accumulations. Excitation of Cm(III) was performed at λ_{ex} = 396.6 nm, which corresponds to the maximum spectral absorbance band of Cm^{3+}(aq). The fluorescence emission was detected by a spectrograph (Shamrock A-SR-303i-B, Andor Technology) with a 300, 600 and 1200 lines/mm grating and an ICCD camera (iStar ICCD, Andor Technology).

The obtained spectra can be interpreted qualitatively by peak position and shape. For a quantitative interpretation, a peak deconvolution and knowledge of the respective pure component spectra is necessary. Single components were extracted by subtracting known pure component spectra from experimentally determined spectra in $MgCl_2$–$Mg(NO_3)_2$ systems.

Results and discussion

Solubility of Nd(III) in dilute to concentrated NaCl–$NaNO_3$, $MgCl_2$–$Mg(NO_3)_2$ and $CaCl_2$–$Ca(NO_3)_2$ solutions

Figure 2 shows examples of the experimental solubility data of $Nd(OH)_3$(s) in 0.10, 0.51, 1.02, 2.64 and 5.61 m NaCl–$NaNO_3$ mixtures obtained in this study (for all data see appendix, Table A.1). Figure 3 shows exemplarily the experimental solubility data of $Nd(OH)_3$(s) obtained in 2.80 m/4.05 m $MgCl_2$–$Mg(NO_3)_2$ mixtures with 1.1 m $\leq m_{NO_3^-} \leq$ 5.8 m and 4.02 m $CaCl_2$–$Ca(NO_3)_2$ mixtures with $m_{NO_3^-}$ = 5.75 m. Solubility data in 0.25 and 1.04 m $MgCl_2$–$Mg(NO_3)_2$, as well as data in 2.80 and 4.05 m $MgCl_2$–$Mg(NO_3)_2$ with $m_{NO_3^-} <$ 1.1 m are provided in Fig. A.1 in the appendix. Figures 2 and 3 also show the experimental solubility data reported by Neck et al. [13] in nitrate-free NaCl, $MgCl_2$ and $CaCl_2$ solutions under analogous pH and ionic strength conditions (except for the system 1.02 m NaCl–$NaNO_3$, which is compared to 0.51 m NaCl reference data). Solubility curves of $Nd(OH)_3$(s) calculated with the thermodynamic and activity models reported by the same authors are also appended in the figures for comparison purposes.

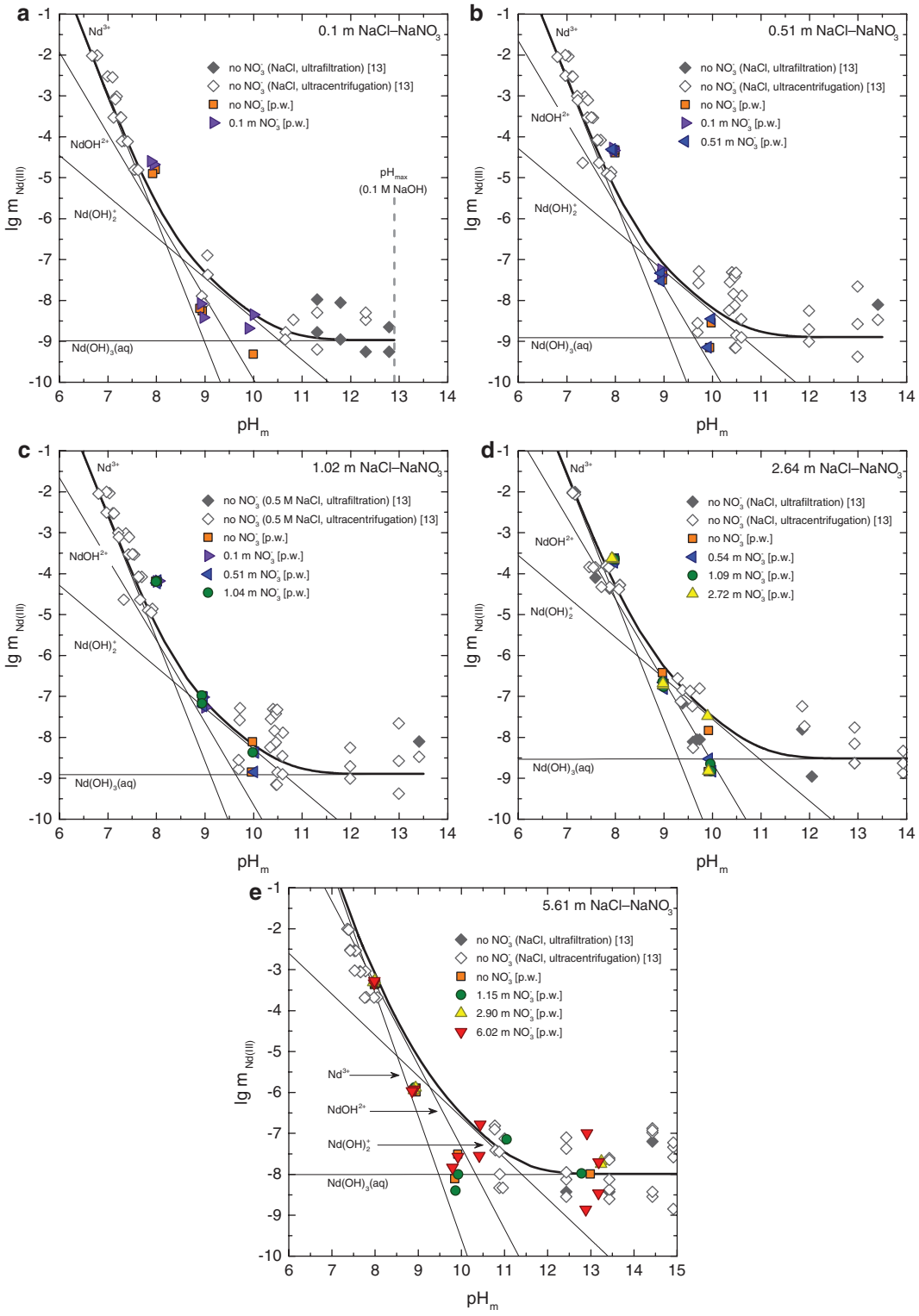

Fig. 2: Solubility of $Nd(OH)_3(s)$ in 0.1–6.02 m NaCl–$NaNO_3$ solutions. Reference data in nitrate-free solutions [13] is included in all the figures for comparison. Thick solid lines correspond to the Nd(III) solubility calculated using thermodynamic and activity models reported in [13] for pure NaCl systems. Thin lines show the aqueous speciation underlying the $Nd(OH)_3(s)$ solubility curve in the same background electrolyte.

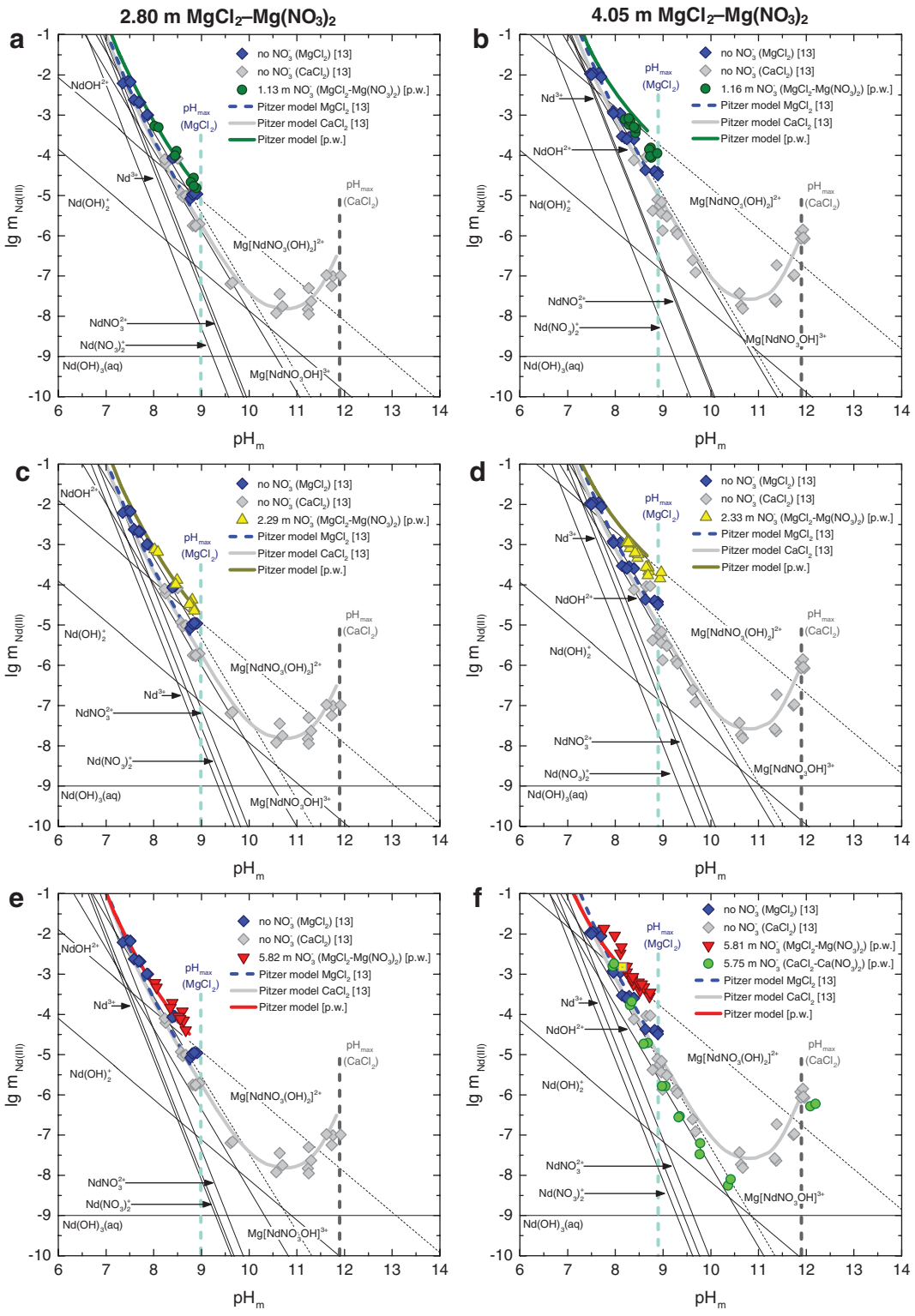

Fig. 3: Solubility of $Nd(OH)_3(s)$ in 2.80 m $MgCl_2$–$Mg(NO_3)_2$ with (a) 1.13 m, (c) 2.29 m and (e) 5.82 m NO_3^- in comparison with 4.05 m $MgCl_2$–$Mg(NO_3)_2$ with (b) 1.16 m, (d) 2.33 m and (f) 5.81 m NO_3^-. The solubility data of $Nd(OH)_3(s)$ in 4.02 m $CaCl_2$–$Ca(NO_3)_2$ with 5.75 m NO_3^- are also included in figure (f). Reference data in nitrate-free solutions [13] is included in all the figures for comparison. Yellow square in (f) indicates the sample used for Nd–L_{III} EXAFS measurements. Thick solid lines correspond to the Nd(III) solubility calculated using thermodynamic and activity models: for pure $MgCl_2$ and $CaCl_2$ systems (blue and grey lines) [13]; for $MgCl_2$–$Mg(NO_3)_2$ mixtures (green, yellow, red lines) [p.w.]. Thin lines show the aqueous speciation underlying $Nd(OH)_3(s)$ solubility curve in $MgCl_2$–$Mg(NO_3)_2$ systems.

No significant effect of nitrate on the solubility of $Nd(OH)_3(s)$ is observed for any of the studied NaCl–$NaNO_3$ systems. On the contrary, these solubility data show a very good agreement with Nd(III) solubility previously reported in nitrate-free NaCl solutions of analogous pH and ionic strength [13], which clearly indicate that no Nd(III)–NO_3 complexation affects solubility in Na–systems with $7.5 \leq pH_m \leq 13.2$.

Nitrate has a negligible effect on the solubility of Nd(III) for the systems 0.25 and 1.04 m $MgCl_2$–$Mg(NO_3)_2$ with nitrate concentrations up to 2.14 m (see appendix, Table A.2). These data are in good agreement with the previously reported $Nd(OH)_3(s)$ solubility in nitrate-free $MgCl_2$ solutions of analogous pH and ionic strength [13]. However, a clear increase in Nd(III) solubility occurs for 2.80 m and 4.05 m $MgCl_2$–$Mg(NO_3)_2$ mixtures and pH_m 8–9 (Fig. 3a–f) compared to the nitrate-free reference data by Neck and co-workers [13]. The increase in solubility becomes more pronounced with increasing nitrate concentration and/or ionic strength. The maximum increase in $Nd(OH)_3(s)$ solubility (about one order of magnitude) is observed in the 4.05 m $MgCl_2$–$Mg(NO_3)_2$ mixture with $m_{NO_3^-} = 5.81$ m (Fig. 3f). The influence of nitrate complexation on the $Nd(OH)_3(s)$ solubility can be shown by comparing experimentally determined Nd(III) concentrations at $pH_m = 8.80$ in 4.05 m $MgCl_2$–$Mg(NO_3)_2$, see Fig. 4. There is a clear and systematic trend to higher Nd(III) solubility with increasing nitrate concentration, e.g., $m_{Nd(III)} = -4.49$ m at $m_{NO_3^-} = 0.24$ m, $m_{Nd(III)} = -4.14$ m at $m_{NO_3^-} = 0.58$ m, $m_{Nd(III)} = -3.93$ m at $m_{NO_3^-} = 1.16$ m, $m_{Nd(III)} = -3.72$ m at $m_{NO_3^-} = 2.33$ m and $m_{Nd(III)} = -3.50$ m at $m_{NO_3^-} = 5.81$ m (Fig. 4). These findings hint to the likely formation of Nd(III)–NO_3 complexes under near-neutral to weakly alkaline pH conditions.

The slope analysis of the experimental solubility data in $MgCl_2$–$Mg(NO_3)_2$ mixtures shows two well-defined pH regions with slope –2 ($pH_m \leq 8.3$) and –1 ($pH_m > 8.3$). This indicates the uptake of 2 and 1 H^+, respectively, in the chemical reaction controlling the solubility of Nd(III) in these pH regions. Based upon a system with solubility controlled by $Nd(OH)_3(s)$ (see next section), the formation of the aqueous species with stoichiometries Nd:OH 1:1 and 1:2 is proposed.

In contrast to the $MgCl_2$–$Mg(NO_3)_2$ system, no significant enhancement in $Nd(OH)_3(s)$ solubility occurs in 2.85 m (see appendix, Table A.3) and 4.02 m $CaCl_2$–$Ca(NO_3)_2$ mixtures with nitrate concentrations up to 5.75 m compared to nitrate-free $CaCl_2$ systems under virtually the same experimental conditions [13]. This observation suggests the likely participation of Mg^{2+} in the formation of Nd(III)–NO_3 complexes in concentrated nitrate bearing $MgCl_2$–$Mg(NO_3)_2$ solutions and pH_m 8–9.

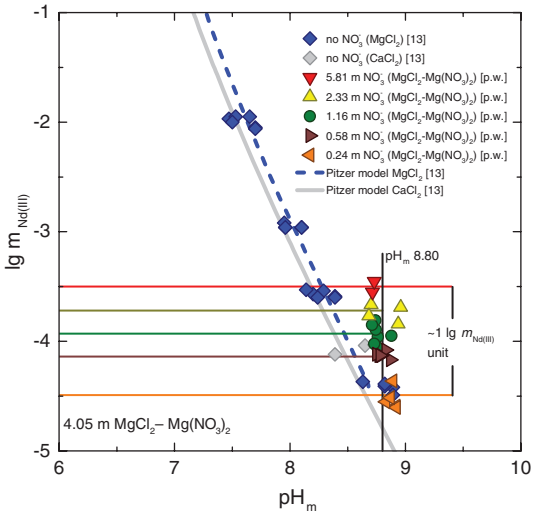

Fig. 4: Solubility of $Nd(OH)_3(s)$ in 4.05 m $MgCl_2$–$Mg(NO_3)_2$ at $pH_m = 8.80$. A clear and systematic trend to higher Nd(III) solubility with increasing nitrate concentration can be seen. The maximum increase in neodymium solubility is about one order of magnitude. Reference data in nitrate-free solutions [13] is included for comparison. Thick solid lines correspond to the Nd(III) solubility calculated using thermodynamic and activity models: for pure $MgCl_2$ and $CaCl_2$ systems (blue and gray lines) [13].

Solid phase characterization in Na–Mg–Cl–NO_3 systems

In all evaluated Na–Mg–Cl–NO_3 systems with $m_{Cl^-} \leq 5.82$ m, the diffractograms of solid phases recovered from selected solubility experiments match the XRD pattern of the initial $Nd(OH)_3$(s) powder (Fig. 5) and are in excellent agreement with the $Nd(OH)_3$(s) reference diffractogram in [21] (PDF 70-0215). Besides $Nd(OH)_3$(s), reflexes belonging to brucite (PDF 74-2220; [30]) and Mg-oxychloride (PDF 07-0412; [31]) initially added to the samples are clearly identified in those solid phases recovered from experiments with $pH_m = pH_{max}$ (data not shown).

A number of solid phases recovered from the solubility experiments in $MgCl_2$–$Mg(NO_3)_2$ solutions were also analyzed by scanning electron microscopy. SEM-EDS analysis show a considerable enrichment of chlorine in Nd(III) solid phases equilibrated with solutions at $m_{Mg^{2+}} \geq 4.05$ m and $m_{Cl^-} \geq 5.82$ m. These results hint towards a solid phase transformation in concentrated chloride brines. A comprehensive study evaluating the formation and stability of Nd(III)–OH–Cl(s) phases is ongoing at KIT–INE.

Cm(III)-TRLFS studies in NaCl–$NaNO_3$, $MgCl_2$–$Mg(NO_3)_2$ and $CaCl_2$–$Ca(NO_3)_2$ solutions

Figure 6a–e shows a selection of experimentally determined Cm(III)–TRLFS spectra in 5.61 m NaCl, 6.02 m $NaNO_3$, 4.05 m $MgCl_2$, 4.05 m $MgCl_2$–$Mg(NO_3)_2$ and 4.02 m $CaCl_2$–$Ca(NO_3)_2$ systems. The Cm^{3+}(aq) reference spectrum measured in a dilute acidic solution is shown in all the figures. All other Cm(III) spectra collected in this work for $MgCl_2$–$Mg(NO_3)_2$ systems are provided in Fig. B.1 in the appendix.

In the absence of other complexing ligands, a number of binary Cm(III) hydroxide, chloride and nitrate species are expected to be present in solution under acidic to weakly alkaline pH conditions. Their relative contribution depends on the pH, ionic strength and electrolyte composition. Wavelengths reported for binary Cm(III)–OH, Cm(III)–Cl and Cm(III)–NO_3 species have been included in the figures for comparison purposes [12, 16, 32–34].

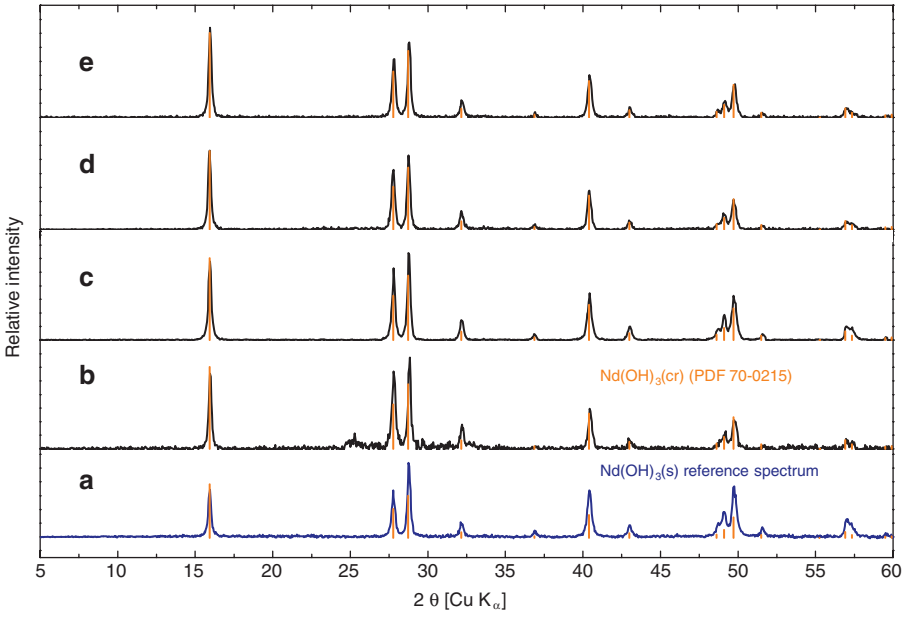

Fig. 5: XRD pattern of Nd(III) solid phases recovered from batch solubility experiments. Initial $Nd(OH)_3$(s) material (a) together with solid phases recovered from experiments in 4.05 m $MgCl_2$–$Mg(NO_3)_2$ with (b) 5.81 m NO_3^- at pH_m 8.43 after 331 days and (c) 2.33 m NO_3^- at pH_m 8.54 after 79 days. Diffractograms (d) and (e) correspond to solid phases recovered from experiments in 2.80 m $MgCl_2$–$Mg(NO_3)_2$ mixtures with 5.82 m NO_3^- at pH_m 8.42 after 331 days and containing no nitrate at pH_m 8.49 after 330 days, respectively.

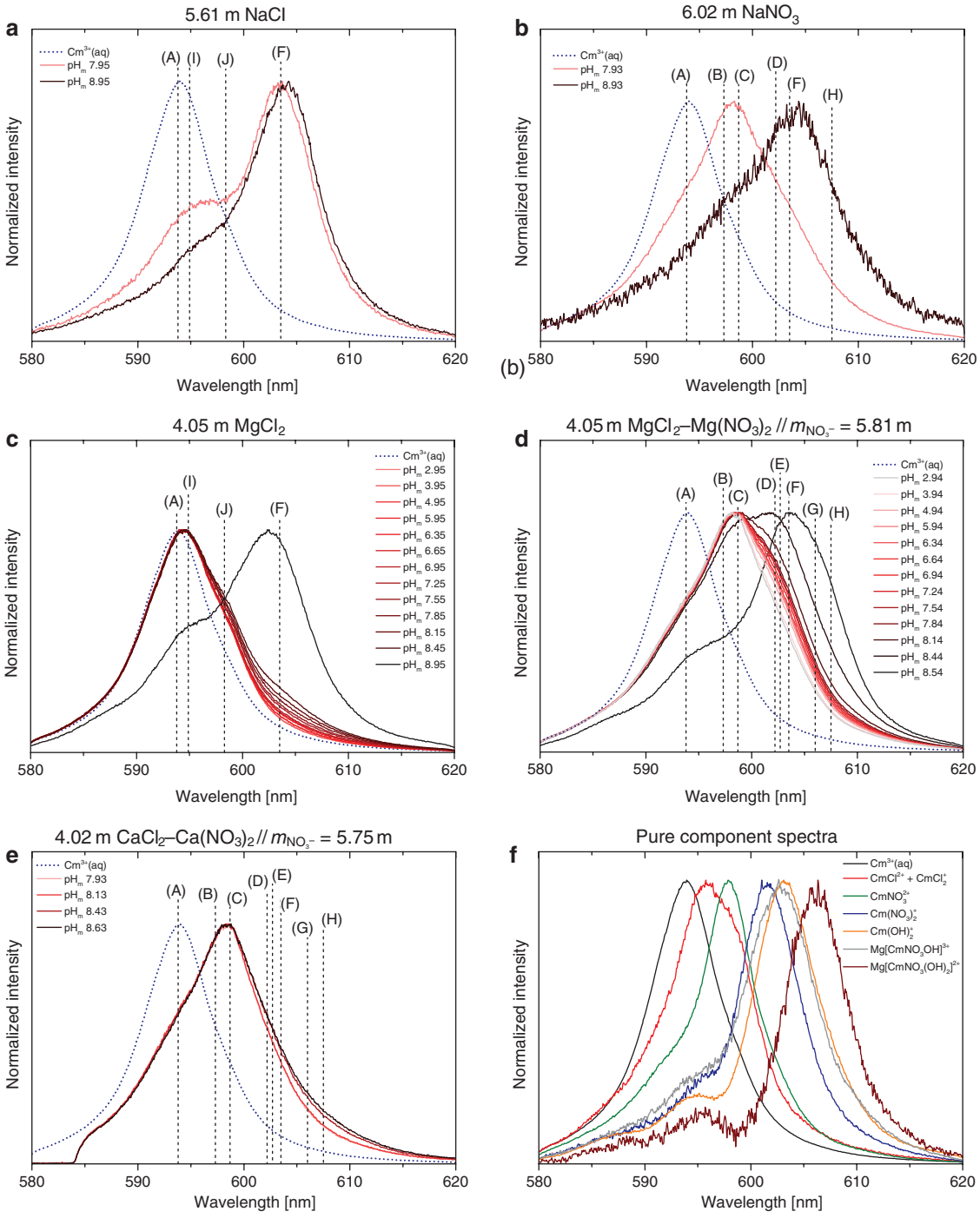

Fig. 6: Selection of experimental Cm(III)–TRLFS spectra over the entire investigated pH range in (a) 5.61 m NaCl, (b) 6.02 m $NaNO_3$, (c) 4.05 m $MgCl_2$, (d) 4.05 m $MgCl_2$–$Mg(NO_3)_2$ mixture with $m_{NO_3^-}$ = 5.81 m and (e) 4.02 m $CaCl_2$–$Ca(NO_3)_2$ mixture with $m_{NO_3^-}$ = 5.75 m. Figure (f) shows all pure component spectra obtained by peak deconvolution of experimental spectra collected in $MgCl_2$–$Mg(NO_3)_2$ systems. Capital letters in figures (a)–(e) refer to: A = Cm^{3+}(aq), B = $CmNO_3^{2+}$, C = $CmOH^{2+}$, D = $Cm(NO_3)_2^{+}$, E = $Mg[CmNO_3OH]^{3+}$, F = $Cm(OH)_2^{+}$, G = $Mg[CmNO_3(OH)_2]^{2+}$, H = $Cm(OH)_3$(aq), I = $CmCl^{2+}$ and J = $CmCl_2^{+}$.

The second Cm(III) hydrolysis species dominate in 5.61 m NaCl (Fig. 6a) over the investigated pH range (between 7.95 and 8.95), whereas binary Cm(III)–NO_3 species prevail in 6.02 m $NaNO_3$ and pH_m = 7.93 (Fig. 6b). At $pH_m \geq 8.93$, $Cm(OH)_2^{+}$ becomes also predominant in 6.02 m $NaNO_3$ (Fig. 6b). The definition of additional

species is not necessary to explain Cm(III) spectra collected in NaCl–$NaNO_3$ solutions, except some minor chloro-species in 5.61 m NaCl.

Cm(III) spectra collected in 4.05 m $MgCl_2$ (Fig. 6c) at $2.95 \leq pH_m \leq 8.45$ are dominated by the Cm^{3+} aquo ion and binary Cm(III)–Cl species, whereas the second hydrolysis species of Cm(III) increases with pH_m and dominates at $pH_m > 8.45$. In the case of the 4.05 m $MgCl_2$–$Mg(NO_3)_2$ system (Fig. 6d), binary Cm(III)–NO_3 species dominate the spectra in the pH range $2.94 \leq pH_m \leq 8.14$. Besides the binary Cm(III)–NO_3 species, additional Cm(III) complexes with a very clear pH dependency form in this system. Peak deconvolution confirms the presence of two new components at $\lambda = 602.7$ nm and $\lambda = 606.0$ nm. These species are absent in pure $MgCl_2$ solutions of the same ionic strength, which clearly indicates the participation of nitrate in the complex formation. The component at $\lambda = 602.7$ nm has been assigned to the moiety "$CmNO_3OH^+$," based on $\lambda(Cm(NO_3)_2^+) = 602.2$ nm [16] and $\lambda(Cm(OH)_2^+) = 603.5$ nm [12, 32, 33], and considering that stronger ligands (e.g., $OH^- > NO_3^-$) induce greater red-shift in the Cm(III) spectra than weaker ones. The strongly red-shifted Cm(III) shoulder at $\lambda = 606.0$ nm has been assigned to the moiety "$CmNO_3(OH)_2(aq)$," taking also as a reference the wavelength reported for the complex $Cm(OH)_3(aq)$ ($\lambda = 607.5$ nm) [12].

The spectra collected in 4.02 m $CaCl_2$–$Ca(NO_3)_2$ (Fig. 6e) differ significantly from the 4.05 m $MgCl_2$–$Mg(NO_3)_2$ system and can be explained considering mainly the formation of binary Cm(III)–NO_3 species with minor contributions of chloro and hydroxo complexes. No mixed Cm(III)–NO_3–OH complexes are observed in relevant concentrations at $pH_m \leq 8.63$. The absence of these species in $CaCl_2$–$Ca(NO_3)_2$ solutions under the same experimental conditions (pH_m, I_m, $m_{NO_3^-}$) as in the $MgCl_2$–$Mg(NO_3)_2$ systems hints towards the participation of Mg^{2+} in the complexation reaction. Consequently, the formation of the quaternary aqueous species $Mg[CmNO_3OH]^{3+}$ and $Mg[CmNO_3(OH)_2]^{2+}$ is proposed and has been considered in the thermodynamic modelling summarized below. Note that under mildly alkaline conditions ($pH_m > 10$) and absence of nitrate, Neck and co-workers [13] proposed the formation of the ternary species $Ca[Cm(OH)_3]^{2+}$ holding the same ligand stoichiometry and charge. These Cm(III)–TRLFS observations are consistent with Nd(III) solubility data under analogous experimental conditions, and thus confirm that the observed increase in solubility for $Nd(OH)_3(s)$ is not caused by ion interaction processes but is related to a genuine Cm(III) complexation reaction with nitrate.

All pure component spectra derived by peak deconvolution using the complete set of TRLFS spectra collected in 4.0 m $MgCl_2$–$Mg(NO_3)_2$ mixtures with $2.93 \leq pH_m \leq 8.95$ and $0.00 \leq m_{NO_3^-} \leq 8.04$ are shown in Fig. 6f.

Nd–L_{III} EXAFS studies in $MgCl_2$–$Mg(NO_3)_2$ solutions

Figure 7 shows the k^2-weighted Nd–L_{III} Fourier transform EXAFS spectrum collected for the supernatant (after 10 kD ultrafiltration) of the Nd(III) solubility sample at $pH_m = 8.15$, 4.05 m $MgCl_2$–$Mg(NO_3)_2$ with 5.81 m NO_3^- (see Fig. 3f). The structural parameters resulting from EXAFS evaluation are shown in Table 3. The best fit

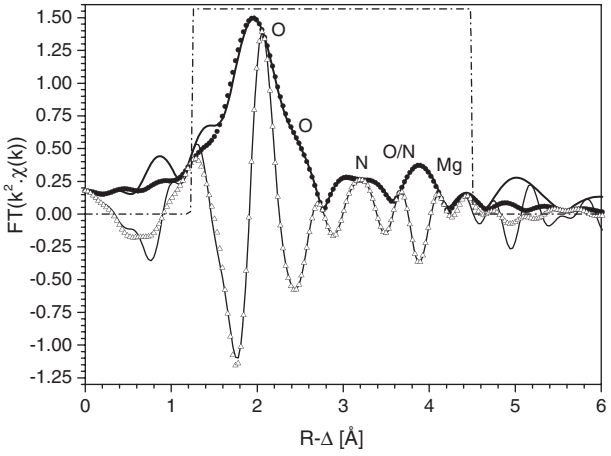

Fig. 7: k^2-weighted Nd–L_{III} Fourier transform EXAFS spectrum of neodymium in 4.05 m $MgCl_2$–$Mg(NO_3)_2$ solution with 5.81 m NO_3^-.

Table 3: Structural parameters obtained from EXAFS evaluation.

Backscatterer	R [Å] (±0.01 Å)	N (±20 %)	σ^2 [Å^2] × 10^{-3}	ΔE_0 [eV]	Goodness of fit (%)
O	2.46	6.1	3.1	8.9	1.0
O	2.64	4.7	3.5		
N	3.18	1.7	3.3		
O/N	3.63	3.6	9.0		
Mg	4.10	2.6	0.4		
O	4.47	4.9	3.5		

R, distances; N, coordination number; σ^2, EXAFS Debye-Waller factors; ΔE_0, relative energy held as global parameters for all atoms; S_0^2 set to 1.

in the FT range [1.25–4.5 Å] is obtained using 6 shells. In addition to O and N shells, a shell with Mg^{2+} as backscatterer is needed to fit the peak at ~4 Å. Furthermore, no Nd–Nd interaction can be evidenced within the R range taken into account. The results point out the presence of one to two nitrate groups, more likely a mixture of species having one and two nitrate groups where at least one of these species has Mg^{2+} in the direct vicinity of OH- and/or NO_3-groups. Further these results are in good agreement with Cm(III)–TRLFS observations in $MgCl_2$–$Mg(NO_3)_2$ mixtures (see Fig. 6d) where under the EXAFS sample characteristics a mixture of binary and quaternary nitrate-bearing aqueous species is expected. In conclusion, Nd–L_{III} EXAFS confirms the formation of quaternary Mg–Nd(III)–NO_3–OH inner-sphere complexes with participation of Mg^{2+} and the absence of polymeric/colloidal Nd(III) species in solution.

Chemical, thermodynamic and activity models

The thermodynamic model derived in [13] for Ln(III) and An(III) in NaCl, $MgCl_2$ and $CaCl_2$ solutions is extended in the present work to nitrate-bearing systems by combining the results from solubility data, spectroscopic techniques and solid phase characterization. $Nd(OH)_3(s)$ is confirmed by XRD and SEM-EDS as solid phase controlling the solubility in all the evaluated systems with $m_{Cl^-} \leq 5.82$ m. The formation of the aqueous species $Mg[An^{III}/Ln^{III}NO_3OH]^{3+}$ and $Mg[An^{III}/Ln^{III}NO_3(OH)_2]^{2+}$ is proposed based on slope analysis, Cm(III)–TRLFS and Nd–L_{III} EXAFS. Hence, equilibrium reactions (1) and (2) can be defined, in combination with equations (3)–(6) for the calculation of the corresponding $\lg^* K'_{s,(1,1,n,1)}$ and $\lg^* K°_{s,(1,1,n,1)}$ with n = 1 or 2.

$$An^{III}/Ln^{III}(OH)_3(s) + 2H^+ + NO_3^- + Mg^{2+} \Leftrightarrow Mg[An^{III}/Ln^{III}NO_3OH]^{3+} + 2H_2O \quad (1)$$

$$An^{III}/Ln^{III}(OH)_3(s) + H^+ + NO_3^- + Mg^{2+} \Leftrightarrow Mg[An^{III}/Ln^{III}NO_3(OH)_2]^{2+} + H_2O \quad (2)$$

with

$$\lg^* K'_{s,(1,1,1,1)} = \lg[Mg[An^{III}/Ln^{III}NO_3OH]^{3+}] - 2\lg[H^+] - \lg[NO_3^-] - \lg[Mg^{2+}] \quad (3)$$

$$\lg^* K'_{s,(1,1,2,1)} = \lg[Mg[An^{III}/Ln^{III}NO_3(OH)_2]^{2+}] - \lg[H^+] - \lg[NO_3^-] - \lg[Mg^{2+}] \quad (4)$$

and

$$\lg^* K°_{s,(1,1,1,1)} = \lg^* K'_{s,(1,1,1,1)} + \lg\gamma_{Mg[An^{III}/Ln^{III}NO_3OH]^{3+}} - 2\lg\gamma_{H^+} - \lg\gamma_{NO_3^-} - \lg\gamma_{Mg^{2+}} + 2\lg a_w \quad (5)$$

$$\lg^* K°_{s,(1,1,2,1)} = \lg^* K'_{s,(1,1,2,1)} + \lg\gamma_{Mg[An^{III}/Ln^{III}NO_3(OH)_2]^{3+}} - \lg\gamma_{H^+} - \lg\gamma_{NO_3^-} - \lg\gamma_{Mg^{2+}} + \lg a_w \quad (6)$$

Provided the very high ionic strength in most of the evaluated systems where the effect of nitrate is observed ($I_m \geq 8.52$ m), the Pitzer formulism has been preferred for the thermodynamic modelling [24]. Parameters reported in [23, 24] are used for the calculation of a_w and the activity coefficients of Mg^{2+}, Cl^-,

Table 4: Equilibrium constants (I = 0, 25 °C) for solid hydroxides and aqueous complexes of Am(III)/Cm(III) and Nd(III).

Solubility: $\lg {}^{*}K^{\circ}_{s,0}$ $[M(OH)_3(s) + 3H^+ \Leftrightarrow M^{3+} + 3H_2O]$			
$Am(OH)_3$(cr/aged)	15.6 ± 0.6 [15]	$Nd(OH)_3$(cr/aged)	16.0 ± 0.4 [35]
$Am(OH)_3$(am)	16.9 ± 0.8 [15]	$Nd(OH)_3$(s)	17.2 ± 0.4 [13]
Hydroxide complexes: $\lg {}^{*}\beta^{\circ}_{1,n}$ $[M^{3+} + nH_2O \Leftrightarrow M(OH)_n^{3-n} + nH^+]$			
$AnOH^{2+}$ (Am/Cm)	−7.2 ± 0.5 [15]	$NdOH^{2+}$	−7.4 ± 0.4 [13]
$An(OH)_2^+$ (Am/Cm)	−15.1 ± 0.7 [15]	$Nd(OH)_2^+$	−15.7 ± 0.7 [13]
$Am(OH)_3$(aq)	−26.2 ± 0.5 [15]	$Nd(OH)_3$(aq)	analogous Am value
$Am(OH)_4^-$	−40.7 ± 0.7 [13]	$Nd(OH)_4^-$	analogous Am value
Chloride complexes: $\lg \beta^{\circ}_{1,q}$ $[M^{3+} + qCl^- \Leftrightarrow MCl_q^{3-q}]$			
$AnCl^{2+}$ (Am/Cm)	0.24 ± 0.03 [15, 36]	$NdCl^{2+}$	analogous Cm value
$AnCl_2^+$ (Am/Cm)	−0.74 ± 0.05 [15, 36]	$NdCl_2^+$	analogous Cm value
Nitrate complexes: $\lg \beta^{\circ}_{1,q}$ $[M^{3+} + qNO_3^- \Leftrightarrow M(NO_3)_q^{3-q}]$			
$AnNO_3^{2+}$ (Cm)	1.33 ± 0.10 [p.w.][a]	$NdNO_3^{2+}$	analogous Cm value
$An(NO_3)_2^+$ (Cm)	1.03 ± 0.10 [p.w.][a]	$Nd(NO_3)_2^+$	analogous Cm value
Mg–M(III)–NO_3–OH complexes: $\lg {}^{*}\beta^{\circ}_{1,1,n,1}$ $[Mg^{2+} + M^{3+} + NO_3^- + nH_2O \Leftrightarrow Mg[MNO_3(OH)_n]^{4-n} + nH^+;\ n = 1, 2]$			
$Mg[AnNO_3OH]^{3+}$ (Am/Cm)	analogous Nd value	$Mg[NdNO_3OH]^{3+}$	−6.4 ± 0.5 [p.w.]
$Mg[AnNO_3(OH)_2]^{2+}$ (Am/Cm)	analogous Nd value	$Mg[NdNO_3(OH)_2]^{2+}$	−15.6 ± 0.5 [p.w.]

[a]Calculated in this work from original experimental data (lg K') in [16].

Table 5: Ion interaction (Pitzer) coefficients for M(III) species (M = Am, Cm, Pu and Nd) in chloride/nitrate media at 25 °C; $\beta^{(0)}_{ik}$, $\beta^{(1)}_{ik}$, λ_{ik} and θ_{ij} in [kg·mol^{-1}], C^{Φ}_{ik} and Ψ_{ijk} in [kg^2·mol^{-2}].

Binary Pitzer parameter					**Ternary Pitzer parameter**			**Refs.**
i	k	$\beta^{(0)}_{ik}$	$\beta^{(1)}_{ik}$	C^{Φ}_{ik}	j	θ_{ij}	Ψ_{ijk}	
M^{3+}	Cl^-/NO_3^-	0.5856	5.60	−0.016	Na^+	0.10	0	[36]
					Ca^{2+}/Mg^{2+}	0.20	0	[36]
MOH^{2+}	Cl^-/NO_3^-	0.055	1.81	0	Na^+	0	0	[40]
					Ca^{2+}/Mg^{2+}	0	0.04	[13]
$M(OH)_2^+$	Cl^-/NO_3^-	−0.13	0	0	Na^+	0	0	[13]
					Ca^{2+}/Mg^{2+}	0.29	0.07	[13]
$M(OH)_3$(aq)	Na^+	λ_{ik} = −0.2						[36]
		λ_{ik} = 0 for k = K^+, Ca^{2+}, Mg^{2+}, Cl^-, NO_3^-, OH^-						[13]
MCl^{2+}	Cl^-/NO_3^-	0.593	3.15	−0.006	Na^+	0	0	[36]
					Ca^{2+}/Mg^{2+}	−0.014	0	[36]
MCl_2^+	Cl^-/NO_3^-	0.516	1.75	0.010	Na^+	0	0	[36]
					Ca^{2+}/Mg^{2+}	−0.196	0	[36]
MNO_3^{2+}	Cl^-/NO_3^-	0.42	1.83	0.050	Na^+	0	0	[p.w.][a]
					Ca^{2+}/Mg^{2+}	0	0	[p.w.][a]
$M(NO_3)_2^+$	Cl^-/NO_3^-	0.25	0.32	0.1	Na^+	0	0	[p.w.][a]
					Ca^{2+}/Mg^{2+}	0	0	[p.w.][a]
$Mg[MNO_3OH]^{3+}$	Cl^-/NO_3^-	0.93	4.30	0	Na^+	0	0	[p.w.]
					Ca^{2+}/Mg^{2+}	0	0	[p.w.]
$Mg[MNO_3(OH)_2]^{2+}$	Cl^-/NO_3^-	0.18	1.60	0	Na^+	0	0	[p.w.]
					Ca^{2+}/Mg^{2+}	0	0	[p.w.]

[a]Calculated in this work from original experimental data (lg K') in [16].

NO_3^- and H^+. Pitzer ion interaction coefficients for Nd(III) species derived in chloride media are reported in [13]. Conditional equilibrium constants reported for binary Cm(III)–NO_3 species at T = 25 °C and 0.10 m ≤ $m_{NO_3^-}$ ≤ 4.61 m (I ≤ 4.61 m) [16] have been used in the present work to determine the corresponding lg β° and ion interaction parameters using the Pitzer approach, see Table 4. For the new species $Mg[An^{III}/$

$Ln^{III}NO_3OH]^{3+}$ and $Mg[An^{III}/Ln^{III}NO_3(OH)_2]^{2+}$, only the binary parameters $\beta^{(0)}$ and the corresponding stability constant at $I = 0$ were calculated. Typical values for analogous cation-anion pairs of the same valence type are used for $\beta^{(1)}$, whereas C^{Φ} was set to 0 [37, 38]. Ternary Pitzer parameters are generally set to 0. The difference between experimental and modelled solubility was minimized by optimizing $\beta^{(0)}$ and $\lg {}^{*}K^{\circ}_{s,(1,1,n,1)}$ for the species $Mg[An^{III}/Ln^{III}NO_3OH]^{3+}$ and $Mg[An^{III}/Ln^{III}NO_3(OH)_2]^{2+}$. A relevant constrain in the modelling exercise is the assumption that ion interaction parameters of cations with Cl^- and NO_3^- are the same. This assumption is based on the very similar solubility of $Nd(OH)_3(s)$ in NaCl–$NaNO_3$ and $CaCl_2$–$Ca(NO_3)_2$ mixtures compared to the nitrate-free reference systems [13] and the very similar SIT ion interaction parameters reported for +1 to +4 monomeric cations [39] (see Fig. C.1 in the appendix). This permits to importantly decrease the number of unknown parameters whilst avoiding relevant variations in the activity coefficients for mixed solutions of same ionic strength but different Cl^-/NO_3^- ratio.

Only solubility data collected for 0.25, 1.04, 2.80 and 4.05 m $MgCl_2$–$Mg(NO_3)_2$ were considered for the optimization exercise, consistently with the validity of the thermodynamic model derived in [13]. Note that solubility samples in pure 4.05 m $Mg(NO_3)_2$ were disregarded in the calculations due to alterations in XRD pattern and SEM-EDS characterization, with respect to the original $Nd(OH)_3(s)$ material. Stability constants and Pitzer ion interaction coefficients resulting from the optimization exercise are shown in Tables 4 and 5, respectively, together with the constants and parameters of all other species and solid phases of relevance in the system Ln^{3+}/An^{3+}–H^+–Na^+–Mg^{2+}–Ca^{2+}–OH^-–Cl^-–NO_3^-–H_2O. Solubility curves and underlying aqueous speciation calculated with the thermodynamic and activity models summarized in Tables 4 and 5 are shown in Figs. 2, 3 and Fig A.1.

Summary and conclusions

The effect of nitrate on the solubility of An^{III}/Ln^{III} was studied in dilute to concentrated NaCl–$NaNO_3$, $MgCl_2$–$Mg(NO_3)_2$ and $CaCl_2$–$Ca(NO_3)_2$ solutions using batch solubility experiments, Cm(III)–TRLFS, Nd–L_{III} EXAFS and extensive solid phase characterization (XRD and SEM-EDS), in order to derive a robust thermodynamic description of repository relevant aqueous systems.

Nitrate has a significant influence on the solubility of $Nd(OH)_3(s)$ in concentrated weakly alkaline $MgCl_2$–$Mg(NO_3)_2$ solutions with total salt concentration ≥ 2.83 m and $m_{NO_3^-} \geq 1.13$ m. However, no effect of nitrate is observed in NaCl–$NaNO_3$ and $CaCl_2$–$Ca(NO_3)_2$ mixtures under analogous experimental conditions, thus indicating the relevant role of Mg^{2+} in the interaction between Nd(III) and nitrate. Cm(III)–TRLFS and Nd–L_{III} EXAFS confirm the participation of Mg^{2+} in the formation of quaternary inner-sphere complexes of the type Mg–An^{III}/Ln^{III}–NO_3–OH.

The combination of slope analyses, TRLFS, EXAFS and solid phase characterization permits to confirm the relevance of the equilibrium reactions $An^{III}/Ln^{III}(OH)_3(s) + H^+ + NO_3^- + Mg^{2+} \Leftrightarrow Mg[An^{III}/Ln^{III}NO_3(OH)_2]^{2+} + H_2O$ and $An^{III}/Ln^{III}(OH)_3(s) + 2H^+ + NO_3^- + Mg^{2+} \Leftrightarrow Mg[An^{III}/Ln^{III}NO_3OH]^{3+} + 2H_2O$ in the control of the solubility of An^{III}/Ln^{III} in concentrated $MgCl_2$–$Mg(NO_3)_2$ brines. Based on the newly generated data, the chemical, thermodynamic and activity models described in [13] for Ln(III) and An(III) are further extended to Ln^{3+}/An^{3+}–H^+–Na^+–Mg^{2+}–Ca^{2+}–OH^-–Cl^-–NO_3^-–H_2O systems.

To our knowledge, this is the first comprehensive experimental study providing a quantitative thermodynamic description of the effect of nitrate on the aquatic chemistry of Ln(III) and An(III) under repository-relevant pH conditions. This study also highlights the key role of spectroscopic techniques in defining correct chemical models of complex systems, especially when involving the formation of "weak complexes" in contraposition to matrix effects or pure ion interaction processes.

Acknowledgments: The authors highly appreciate the technical contribution by M. Böttle, N. Finck, F. Geyer and E. Soballa of KIT-INE. The valuable comments by V. Metz (KIT-INE) and three anonymous reviewers significantly contributed to the improvement of this manuscript are gratefully acknowledged.

References

[1] V. Metz, H. Geckeis, E. Gonzalez-Robles, A. Loida, C. Bube, B. Kienzler. *Radiochim. Acta* **100**, 699 (2012).
[2] S. K. Frape, P. Fritz. *Geochim. Cosmochim. Ac.* **48**, 1617 (1984).
[3] W. Brewitz. *GSF-T 114*, Ges. f. Strahlen- u. Umweltforschung, Braunschweig (1980).
[4] C. Bube, V. Metz, E. Bohnert, K. Garbev, D. Schild, B. Kienzler. *Phys. Chem. Earth* **64**, 87 (2013).
[5] A. P. Paiva, P. Malik. *J. Radioanal. Nucl. Chem.* **261**, 485 (2004).
[6] B. A. Crawford, S. A. Lott, L. D. Sparks, G. Van Soest, B. McInroy. In *Waste Management 2006 Conference, WM'06 Conference*, Tucson, Arizona (2006).
[7] D. C. Kicker, C. G. Herrick. WIPP:1.2.5:PA:QA-L:559199, Carlsbad (2013).
[8] R. C. Philip Hill. WRPS-49044-FP, Richland (2011).
[9] L. Truche, G. Berger, A. Albrecht, L. Domergue. *Appl. Geochem.* **28**, 155 (2013).
[10] M. Altmaier, X. Gaona, T. Fanghänel. *Chem. Rev.* **113**, 901 (2013).
[11] M. Altmaier, V. Neck, T. Fanghänel. *Radiochim. Acta* **96**, 541 (2008).
[12] T. Rabung, M. Altmaier, V. Neck, T. Fanghänel. *Radiochim. Acta* **96**, 551 (2008).
[13] V. Neck, M. Altmaier, T. Rabung, J. Lützenkirchen, T. Fanghänel. *Pure Appl. Chem.* **81**, 1555 (2009).
[14] D. Fellhauer, V. Neck, M. Altmaier, J. Lützenkirchen, T. Fanghänel. *Radiochim. Acta* **98**, 541 (2010).
[15] R. Guillaumont, T. Fanghänel, V. Neck, J. Fuger, D. A. Palmer, I. Grenthe, M. H. Rand. *Chemical Thermodynamics Vol. 5. Update on the Chemical Thermodynamics of Uranium, Neptunium, Plutonium, Americium and Technetium*, Elsevier, Amsterdam (2003).
[16] A. Skerencak, P. J. Panak, W. Hauser, V. Neck, R. Klenze, P. Lindqvist-Reis, T. Fanghänel. *Radiochim. Acta* **97**, 385 (2009).
[17] L. Rao, G. Tian. *Dalton Trans.* **40**, 914 (2011).
[18] W. Hummel. Report AN-44-01-28, Villigen (2001).
[19] W. Hummel, G. Anderegg, L. Rao, I. Puigdomenech, O. Tochiyama. *Chemical Thermodynamics Vol. 9. Chemical Thermodynamics of Compounds and Complexes of U, Np, Pu, Am, Tc, Se, Ni and Zr with Selected Organic Ligands*, Elsevier, Amsterdam (2005).
[20] I. Grenthe, F. Mompean, K. Spahiu, H. Wanner. *Guidelines for the Extrapolation to Zero Ionic Strength*, OECD-NEA, Issy-les-Moulineaux (2013).
[21] G. W. Beall, W. O. Milligan, D. R. Dillin, R. J. Williams, J. J. McCoy. *Acta Crystallogr. Sec. B* **32**, 2227 (1976).
[22] M. Altmaier, V. Metz, V. Neck, R. Müller, T. Fanghänel. *Geochim. Cosmochim. Acta* **67**, 3595 (2003).
[23] C. E. Harvie, N. Moller, J. H. Weare. *Geochim. Cosmochim. Ac.* **48**, 723 (1984).
[24] K. S. Pitzer. *Activity Coefficients in Electrolyte Solutions*, CRC Press, Boca Raton (1991).
[25] M. Weiser, T. Rabung, H. Geckeis. In *13th International Conference on the Chemistry and Migration Behaviour of Actinides and Fission Products in the Geosphere, MIGRATION'11*, pp. 62–63, Beijing, China (2011).
[26] JCPDS. Powder diffraction files. Joint Commitee on Powder Diffraction Standards, Swarthmore, USA (2001).
[27] B. Ravel, M. Newville. *J. Synchrotron Radiat.* **12**, 537 (2005).
[28] D. F. Mullica, E. L. Sappenfield, D. A. Grossie. *J. Solid State Chem.* **63**, 231 (1986).
[29] D. J. Rogers, N. J. Taylor, G. E. Toogood. *Acta Cryst.* **39**, 939 (1983).
[30] G. Isetti. *Period. Mineral.* **34**, 327 (1965).
[31] P. M. de Wolff. *Technisch Physische Dienst*, Delft (1957).
[32] T. Fanghänel, J. I. Kim, P. Paviet, R. Klenze, W. Hauser. *Radiochim. Acta* **66/67**, 81 (1994).
[33] T. Fanghänel, J. I. Kim. *J. Alloy Compd.* **271–273**, 728 (1998).
[34] T. Fanghänel, J. I. Kim, R. Klenze, Y. Kato. *J. Alloy Compd.* **225**, 308 (1995).
[35] I. I. Diakonov, B. R. Tagirov, K. V. Ragnarsdottir. *Radiochim. Acta* **81**, 107 (1998).
[36] T. Könnecke, T. Fanghänel, J. I. Kim. *Radiochim. Acta* **76**, 131 (1997).
[37] I. Grenthe, A. Plyasunov. *Pure Appl. Chem.* **69**, 951 (1997).
[38] A. Plyasunov, T. Fanghänel, I. Grenthe. *Acta Chem. Scand.* **52**, 250 (1998).
[39] M. H. Rand, J. Fuger, I. Grenthe, V. Neck, D. Rai. *Chemical Thermodynamics Vol. 11. Chemical Thermodynamics of Thorium*, OECD Publications, Paris (2008).
[40] V. Neck, T. Fanghänel, J. I. Kim. Report FZKA 6110, Karlsruhe (1998).

Supplemental Material: The online version of this article (DOI: 10.1515/pac-2014-1205) offers supplementary material, available to authorized users.